Journal of Applied Polymer Science

Double-Nozzle Air-Jet Electrospinning for Nanofiber Fabrication

Congcong Pu,[1] Jianxin He,[2] Shizhong Cui,[1,2] Weidong Gao[1]

[1]School of Textile & Clothing, Jiangnan University, Wuxi 214122, People's Republic of China

[2]Key Laboratories of Functional Textiles of Henan Province, Zhongyuan University of Technology, Zhengzhou 450007, People's Republic of China

Correspondence to: J. X. He, College of Textiles, Zhongyuan University of Technology, 41 Zhongyuan Road, P. O. Box 110, Zhengzhou City, Henan Province 450007, People's Republic of China (E-mail: hejianxin771117@163.com)

ABSTRACT: A novel double-nozzle air-jet electrospinning apparatus was developed to fabricate nanofibers on a large scale. The distribution of the electric field at different nozzle distances was simulated to analyze the jet path, productivity, and deposition area of nanofiber webs and the nanofiber morphology. Our experiments showed that the bubbles usually ruptured intermittently on the top surface of the two nozzles and the jets traveled in a straight path with a high initial velocity. A continuous and even thickness of the nanofiber webs were obtained when the nozzle distances was less than 55 mm. At nozzle distances of 55 mm, the received fibers were thin with the lowest standard deviation. Experimental parameters involving the applied voltage, collecting distance, and air flow rate were also investigated to analyze the nanofiber morphology at a nozzle distance of 55 mm. The results show that the nanofibers presented a finer and thinner diameter at an applied voltage of 36 kV, a collecting distance of 18 cm, and an air flow rate of 800 mL/min. The nanofiber production of this setup increased to nearly 70 times that with a single-needle electrospinning setup. On the basis of the principle of this air-jet electrospinning setup, various arrangements of multinozzle electrospinning setups could be designed for higher throughput of nanofibers. © 2013 Wiley Periodicals, Inc. J. Appl. Polym. Sci. **2014**, *131*, 40040.

KEYWORDS: electrospinning; fibers; theory and modeling

Received 22 April 2013; accepted 6 October 2013
DOI: 10.1002/app.40040

INTRODUCTION

Electrospinning has been recognized as a feasible technique for nanofiber fabrication. Recently, various materials of nanofiber webs have been successfully electrospun for several potential applications, including tissue engineering scaffolds, filters, drug-delivery materials, and self-cleaning textiles.[1,2] However, these applications were somewhat limited by the low production rate of the single-needle electrospinning (SNE) setup.[3] Although considerable work on multineedle electrospinning[4,5] has been done to improve nanofiber productivity, some challenges caused by jet repulsion from neighboring jets still exist; these include separation and uneven thickness of nanofiber webs and the complex design for the multineedle setup.[6] Particularly, small needle diameters led to needle blocking.[7] Varesano et al.[8] reported multineedle electrospinning in which the process perturbation phenomenon of jets occurred; this resulted in defects in the nanofiber webs and failure to produce fibrous materials. The effects of the electric field on the multijet and fiber morphology were investigated by Angammana and Jayaram.[9] However, at small needle distances, the jets traveled with a vertical angle because of jet repulsion, and this resulted in a separated deposition area of the nanofiber mats.

To overcome the problem of jet repulsion, researchers have created many effects by controlling the shape and the strength of the electric field. For example, charged metal walls that carried the same type charges with multiple needles were used by Liu et al.[10] to suppress jet repulsion. As a result, a small deposition spot size was obtained. However, repulsion was only suppressed slightly with an increase in the needle number. Positively charged rings were used by Kim et al.[11] to dampen the jet repulsive instability and control the deposition area of nanofiber webs, but no further explanation for this result has been made. Although experimental observations showed that repulsive interference of multijets could be weakened through an increase in the needle spacing,[12] effective methods to solve multijet repulsion and obtain continuous and even nanofiber webs have not been proposed. Needleless electrospinning, developed to improve the productivity of nanofibers, can be divided into rotating spinneret electrospinning and stationary spinneret electrospinning.[13,14] Rotating spinneret electrospinning includes the use of spiral coils,[15] discs,[16] and cylinders[17] as spinnerets. However, these setups need a high critical voltage of 60 kV to be applied for electrospinning. Other needleless electrospinning methods of stationary spinneret electrospinning have mainly

involved bubble electrospinning,[18] splashing electrospinning,[19] and conical wire coil electrospinning.[13] Bubble electrospinning is considered as convenient method for the mass production of nanofibers, but the open solution supply system results in changes in the solution concentration.[18] On the basis of the principle of energy conservation, a lower electrospun critical voltage is needed for bubble electrospinning because additional forces facilitate jet initiation.

A novel double-nozzle air-jet electrospinning device was developed to scale up nanofiber production on the basis of the principle that one bubble can rupture into a multijet for electrospinning.[20] This device has many special advantages, such as a stable concentration of the electrospun solution, the ability to produce more uniform and thinner fibers,[19] high throughputs with lower critical voltages,[15–17] easy assembly with simple operation, and the control of the jet-formed speed and position. The effects of the electric field on the jet path, productivity, web deposition, and fiber morphology were investigated when the nozzle distance was changed. In addition, at a nozzle distance of 55 mm, experimental parameters, such as the applied voltage, collecting distance, and air flow rate, were also investigated to determine the nanofiber morphology.

EXPERIMENTAL

Preparation of the Electrospinning Solution

Polyacrylonitrile (PAN) with an average molecular weight of 60,000 Da was purchased from China Hangzhou Acrylon Co., Ltd. *N,N*-Dimethylformamide (DMF) was purchased from China Shanghai Aldrich-Sigma Co., Ltd., and was used as received. The polymer was dried at 100°C *in vacuo* for 2 h before use. The 16% PAN solution with DMF was prepared at a room temperature of 80°C for 4 h under a constant mixing speed as an electrospun solution.

Double-Nozzle Electrospinning Setup

The double-nozzle air-jet electrospinning apparatus is schematically shown in Figure 1(a). As shown in this figure, the electrospinning apparatus used in this study consisted of the double-nozzle spinneret, the collector, the high-voltage generator, the solution supply system, and the air supply system. The cylinder single nozzle spinneret shown in Figure 1(b) consisted of a partly conductive spray nozzle in which the polymer solution was stored, a gas storage chamber, and a gas-guide tube that was arranged coaxially to and below the top of the surface of the spray nozzle, a liquid transportation pipe, and a gas transportation pipe. The inner diameter of the spray nozzle was 30 mm, and the inner diameter of the gas-guide tube was half that of the spray nozzle.

Electrospinning Process

During electrospinning, air was transported by the two sides' air pumps into the gas storage chambers of the two nozzles.

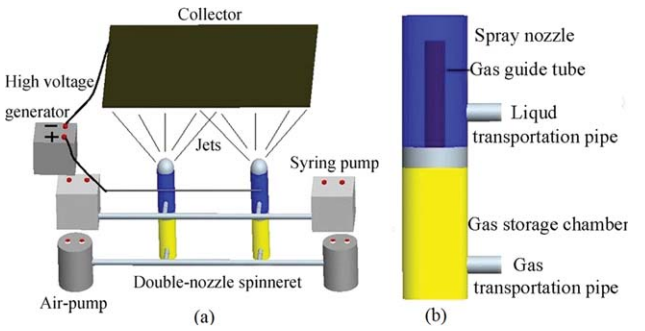

Figure 1. (a) Schematic diagram of the double-nozzle air-jet electrospinning setup. (b) Structure chart of the double-nozzle spinneret. [Color figure can be viewed in the online issue, which is available at wileyonlinelibrary.com.]

After that, the solution was transported by the two sides' syringe pumps into the liquid storage chambers of the two nozzles. As a result, bubbles formed intermittently on the top surface of the two nozzles. The electrospinning setup was charged by a direct-current, high-voltage generator, and the collector was grounded. Once the applied electric field overcame the surface tension, one bubble burst into multiple jets, which were stretched and subsequently produced nanofibers on the collector. By adjusting the flow velocity of the air, one can control the formed frequency and the shape of the bubbles precisely.

In this experiment, the nozzle distance was varied from 20 to 65 mm to investigate the jet path, productivity, deposition area of the nanofiber webs, and nanofiber morphology. The polymer solution was electrospun at a positive voltage of 36 kV and a tip-to-collector distance of 18 cm. The flow rate of the solution for a single nozzle was 9 mL/h, and the flow rate of air for a single nozzle was 800 mL/min. In addition, at a nozzle distance of 55 mm, the electrospinning parameters, such as the applied voltage, collecting distance, and air flow rate, were also investigated for nanofiber morphology. The experimental conditions during the spinning process are shown in Table I.

Electric Field Analysis

The electric field was calculated by a finite element method with Ansoft Maxwell 12 two-dimensional (2D) and three-dimensional (3D) software. The solution type was set as electrostatic in our simulation. The double nozzle and collector were transformed into geometrical objects in Ansoft Maxwell, and their practical dimensions, locations, and relative permittivity were input. The collector was made of aluminum, and its bulk conductivity was 1.1×10^6 Siemens/m. The top part of the spray nozzle was made of stainless steel, and its bulk conductivity was 3.8×10^7 Siemens/m. The left part of the spray nozzle

Table I. Processing Parameters of Electrospinning

PAN/DMF solution (% by weight)	Nozzle distances (mm)	Spinning voltages (kV)	Spinning distances (cm)	Flow rates of air (mL/min)
16	20, 40, 55, 65	24, 28, 32, 36	14, 16, 18, 20	400, 600, 800, 1000

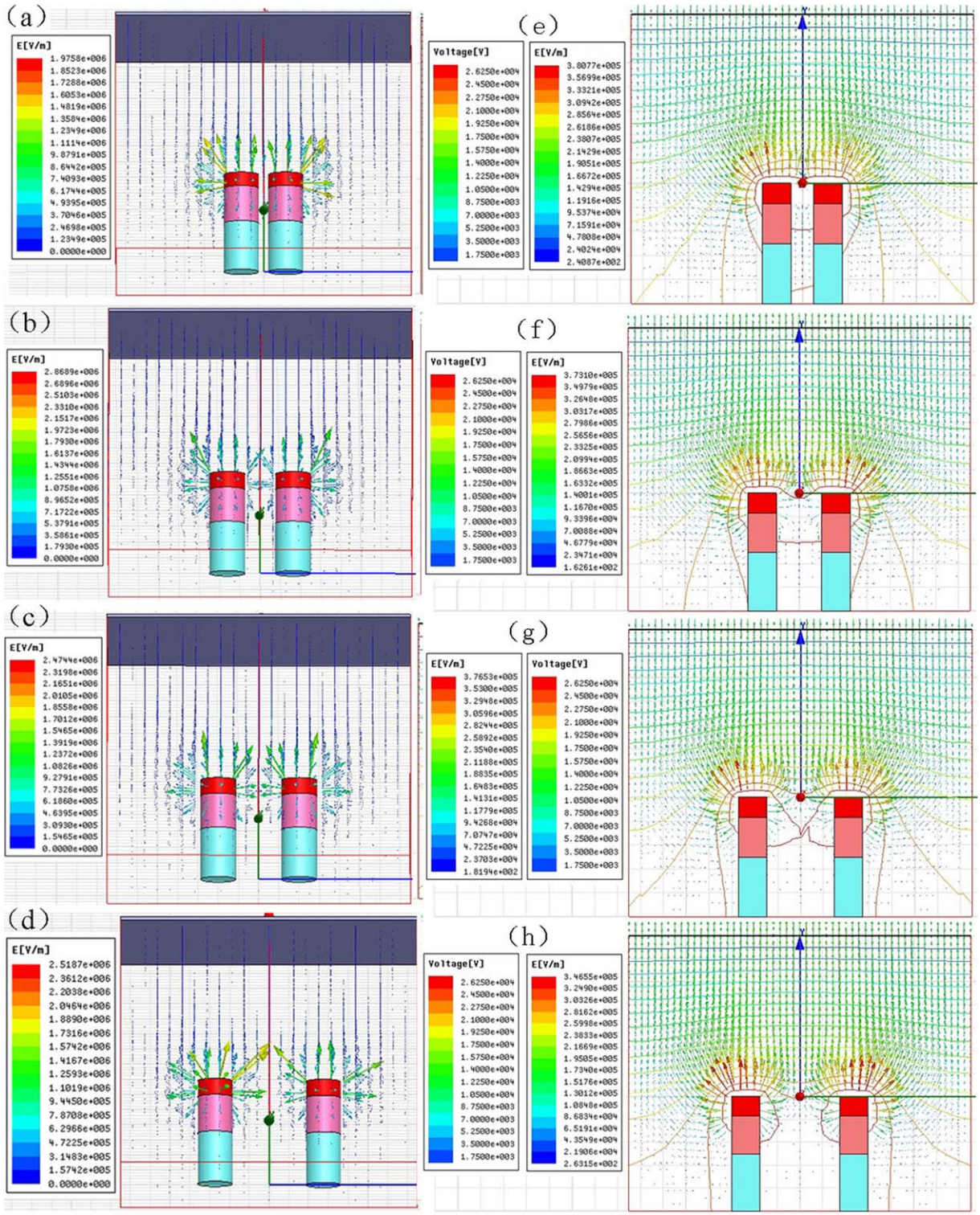

Figure 2. Simulation results of the double-nozzle air-jet electrospinning setup of the 3D models at nozzle distances of (a) 20, (b) 40, (c) 55, and (d) 65 mm and 2D models at nozzle distances of (e) 20, (f) 40, (g) 55, and (h) 65 mm. [Color figure can be viewed in the online issue, which is available at wileyonlinelibrary.com.]

was made of an insulating material, and its bulk conductivity was 0. The relative permittivity of these materials was 1. The excitation source of the voltage instead of the boundary conditions was assigned. The voltage of the nozzles and collector were set as 36 and 0 kV, respectively, and these parameters were set as the matrix. The simulation results of the electric field were formed after the adaptive meshing process and the solving process of the program.

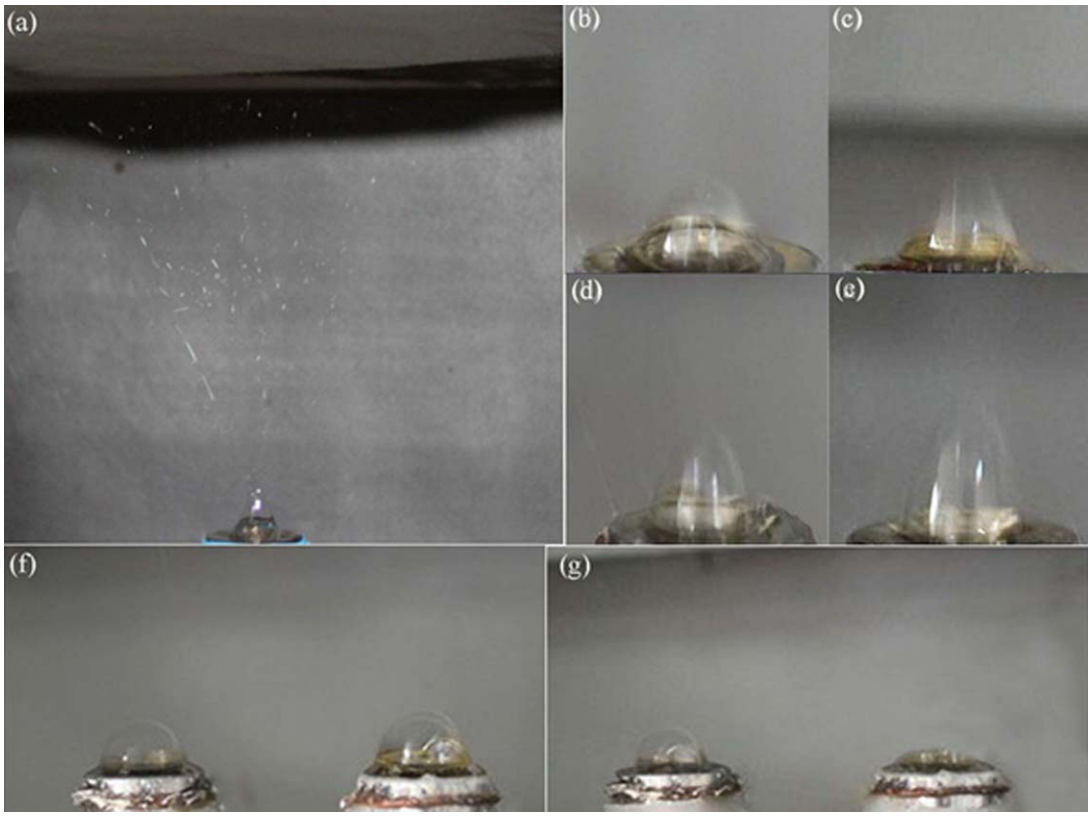

Figure 3. Photographs of double-nozzle air-jet electrospinning: (a) process of air-jet electrospinning; (b–e) views of the bubbles at nozzle distances of (b) 20, (c) 40, (d) 55, and (e) 65 mm; and (f,g) two views of bubbles formed on the top surface of the nozzles. [Color figure can be viewed in the online issue, which is available at wileyonlinelibrary.com.]

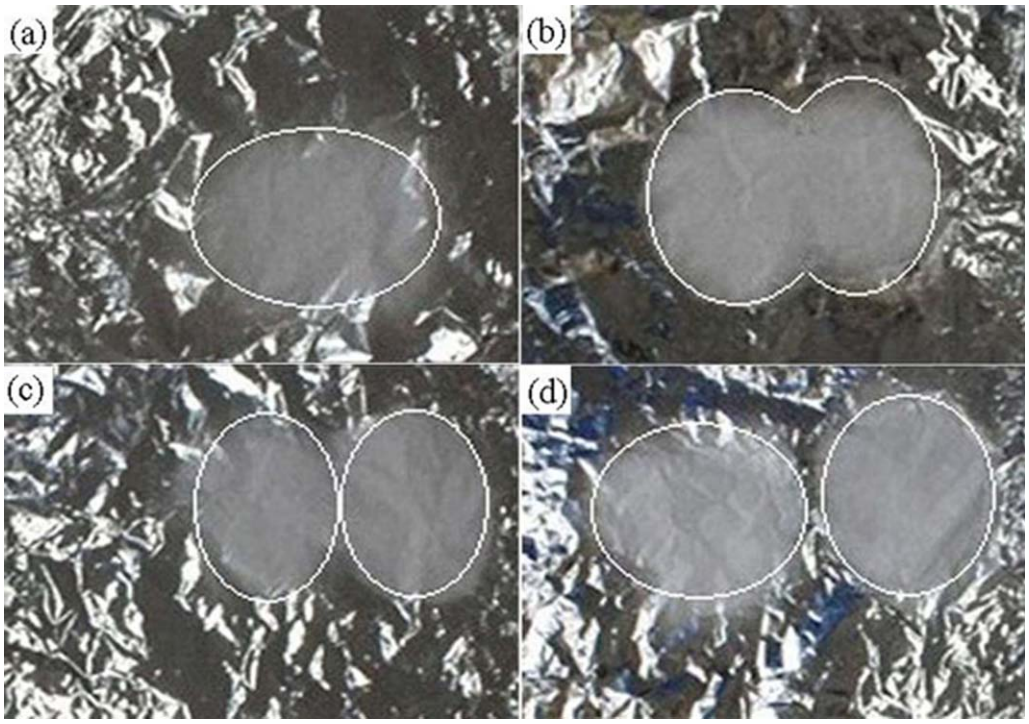

Figure 4. Photographs of nanofiber webs produced by double-nozzle air-jet electrospinning at nozzle distances of (a) 20, (b) 40, (c) 55, and (d) 65 mm. [Color figure can be viewed in the online issue, which is available at wileyonlinelibrary.com.]

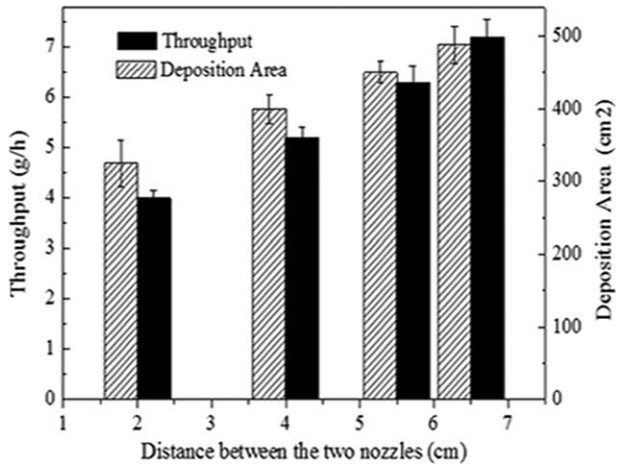

Figure 5. Productivity and deposition area of nanofiber webs produced by the double-nozzle air-jet electrospinning setup at different nozzle distances.

Characterization

The area for collecting the nanofiber webs was 30 × 30 mm^2, and the time was 10 min. The surface morphology of the PAN nanofibers was characterized with a scanning electron microscope (JSM-6360LVSEM, JEOL Co., Japan) at an accelerating voltage of 15 kV. Before they were scanned with scanning electron microscopy (SEM), the samples were sputter-coated for 90 s with gold. More than 100 nanofibers from different SEM images were taken to measure the diameter and standard deviation (SD) with Nano Measurer 1.2 software. The jet path charged with different positive electrodes was observed by a EOS 500 D Canon digital camera.

RESULTS AND DISCUSSION

Electric Field Simulation at Different Nozzle Distances

3D models of the double nozzle were created to simulate an electric field at different nozzle distances with the Ansoft Maxwell software [Figure 2(a–d)]. At the same time, 2D

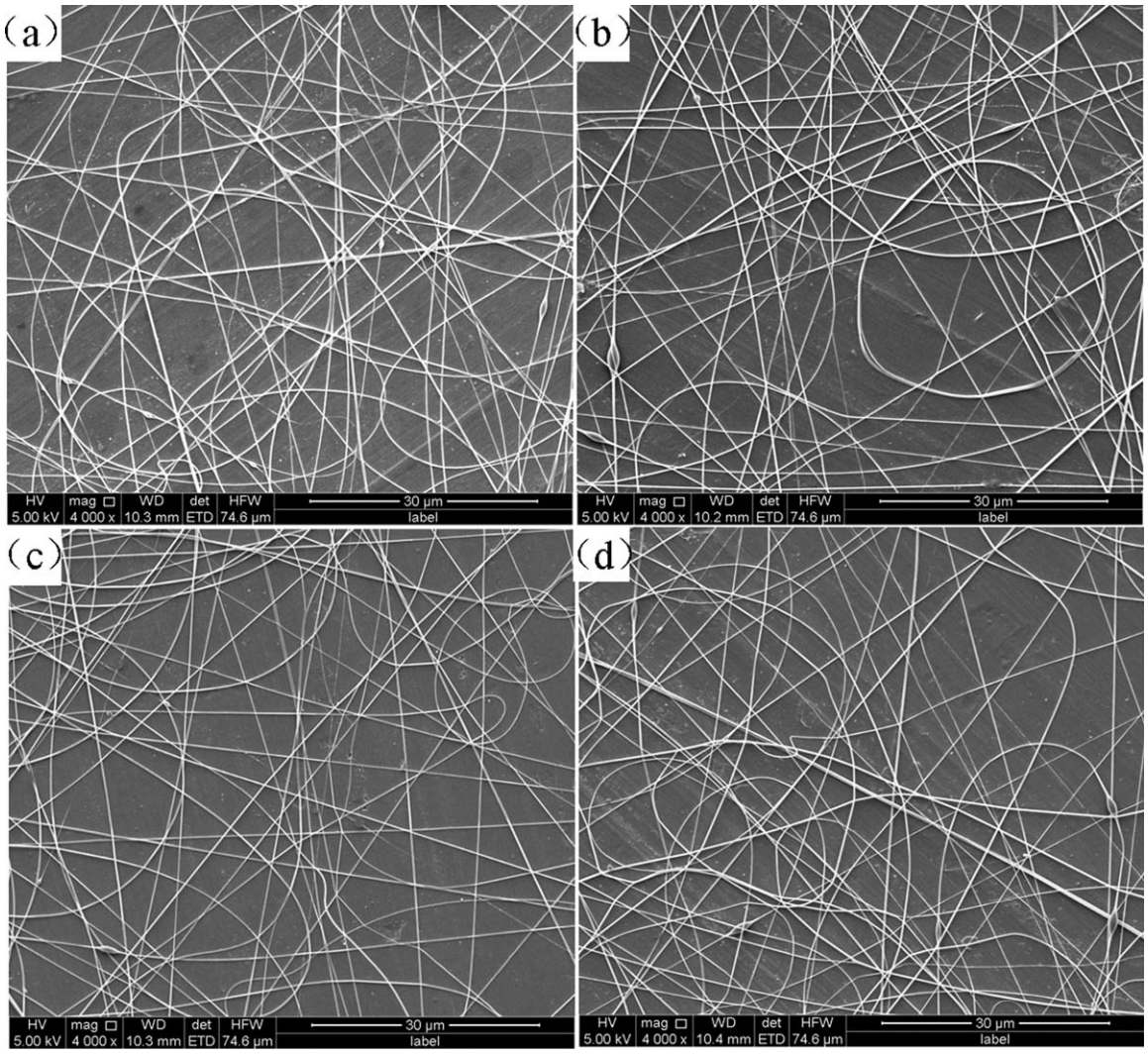

Figure 6. SEM micrographs of nanofibers produced by the double-nozzle air-jet electrospinning setup at nozzle distances of (a) 20, (b) 40, (c) 55, and (d) 65 mm.

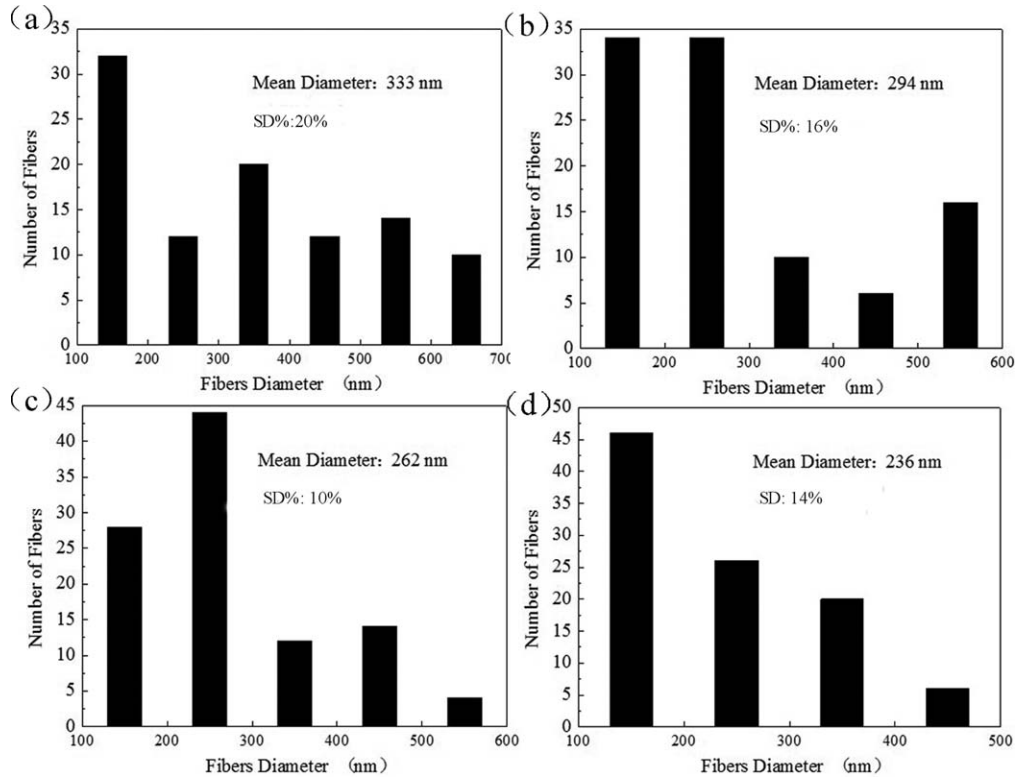

Figure 7. Average diameters and SDs of nanofibers produced by the double-nozzle air-jet electrospinning setup at nozzle distances of (a) 20, (b) 40, (c) 55, and (d) 65 mm.

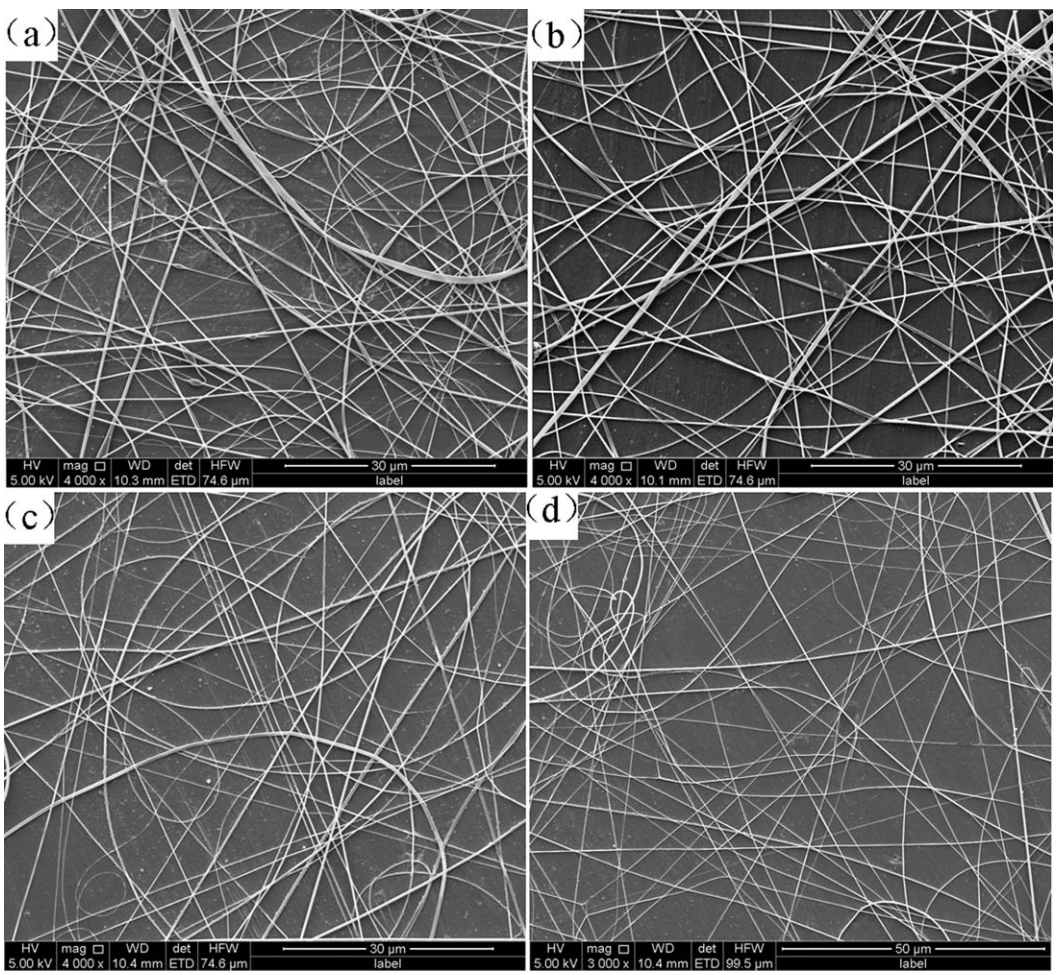

Figure 8. SEM micrographs of nanofibers produced at applied voltages of (a) 24, (b) 28, (c) 32, and (d) 36 kV.

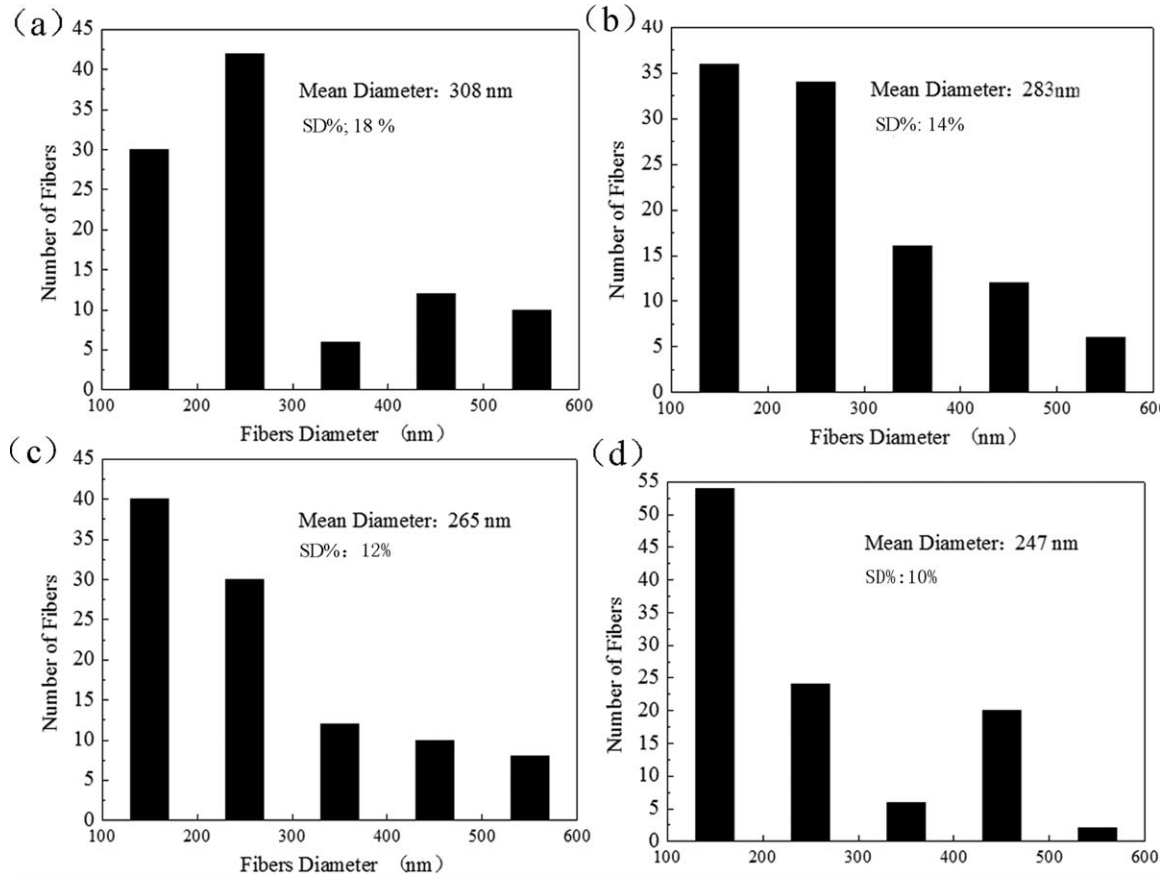

Figure 9. Histograms showing the size distributions and SDs of nanofibers at applied voltages of (a) 24, (b) 28, (c) 32, and (d) 36 kV.

models that passed through the axis of the nozzles and the collector were also created to simulate an electric field at different nozzle distances [Figure 2(e–h)]. The arrows are the electric field vectors, which denote the direction and distribution of the electric field.[21] The lengths of the arrows provide a quantitative indication of the strength of the electric field. The equipotential lines are perpendicular to the electric field lines.

When the nozzle distances were 20 and 40 mm, the equipotential lines of the two nozzles were enclosed; this indicated that the interaction of the electric field between the two nozzles was strong [Figure 2(e,f)]. As shown in Figure 2(g,h), the enclosed equipotential lines began to separate; this indicated that the interaction of the electric field could be neglected when the nozzle distances exceeded 55 mm. The length of the arrows indicate that the electric field was more uniformly distributed at a nozzle distance of 55 mm [Figure 2(c,g)]. With increasing nozzle distance, the distance from the paralleled equipotential lines to the top surface of the two nozzles became closer [Figure 2(e–h)].

The electric intensity of the nozzles was different at different nozzle distances because of the changed interaction of the electric field. As shown in Figure 2(a,b), when the nozzle distance increased from 20 to 40 mm, the interaction of the electric field was weakened; this led to the enhancement of the electric field in the middle of two nozzle planes. However, when the nozzle distance exceeded 55 mm, the electric field in the middle of the two nozzle planes decreased gradually because of the separated equipotential lines [Figure 2(c,g)]. Meanwhile, when the nozzle distance increased from 40 to 65 mm, the interaction of the electric field was weakened, and this resulted in an enhanced electric field on the top of each nozzle [Figure 2(a–d)]. Otherwise, with the increase in the nozzle distance, the electric field strength at the two sides of the nozzles became stronger, and more electric field lines were perpendicular to the collector (Figure 2). These modeling results could be used to explain the experimental data.

Nanofiber Fabrication at Different Nozzle Distances

In the traditional electrospinning process, the solution droplet is first stretched by the electrostatic force into a Taylor cone. When the electrostatic force exceeds a critical value, the cone is stretched into one jet, which undergoes a series of repulsive instability to produce nanofibers. Photograph of the jets for air-jet electrospinning are shown in Figure 3(a). When the voltage exceeded a critical value, one bubble could burst into a multijet under the action of the electrostatic force and the internal pressure in the bubble. Therefore, the productivity of the nanofibers was enhanced compared to that obtained with the SNE setup. Because of

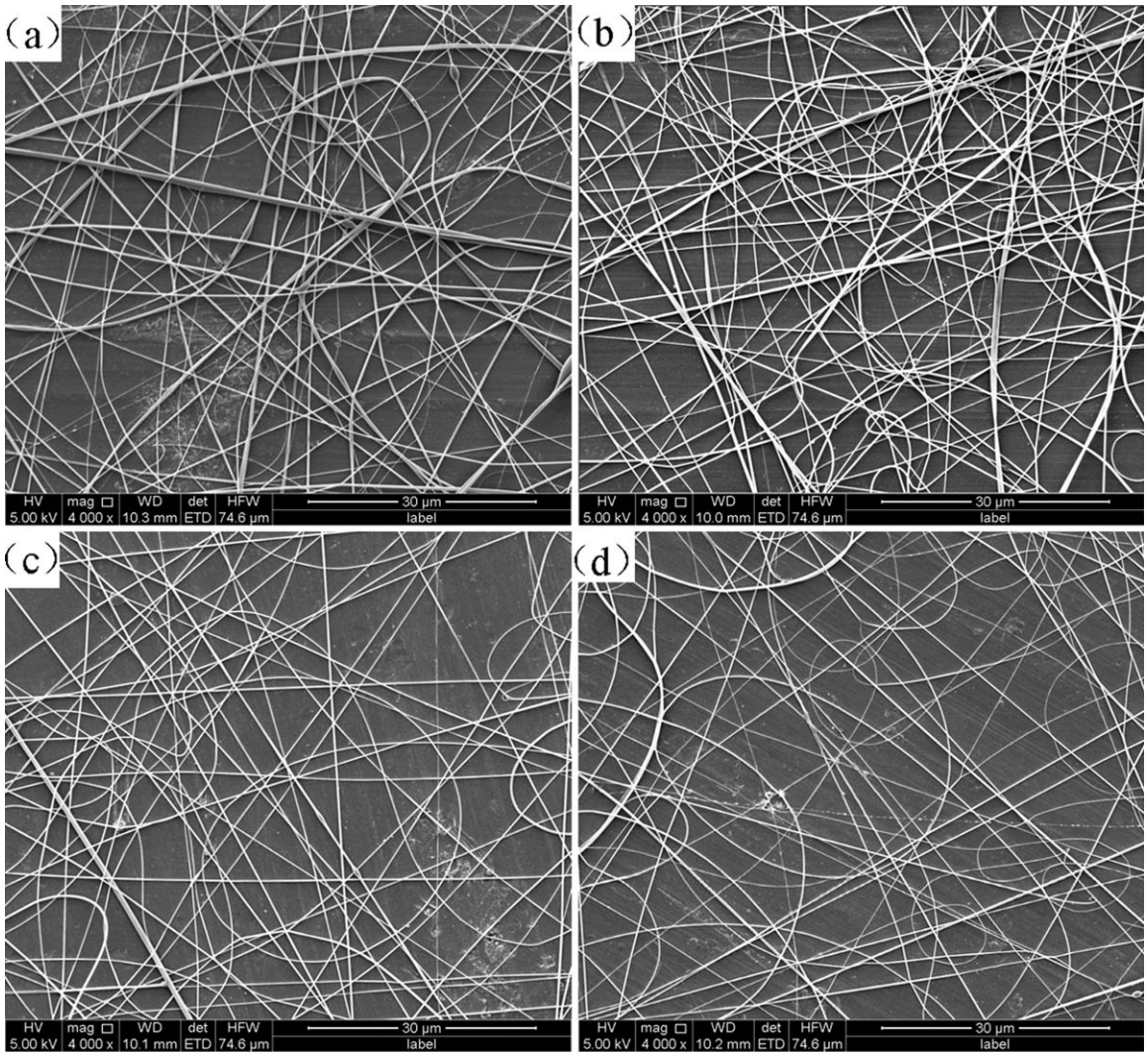

Figure 10. SEM micrographs of nanofibers produced at nozzle distances of (a) 14, (b) 16, (c) 18, and (d) 20 cm.

the effects of the internal pressure in the bubble, the jets from the ruptured bubble traveled a straight path with a high initial velocity. Therefore, the repulsive instability of the jets hardly occurred before the jets reached the collector. The shapes of the bubbles at different nozzle distances are shown in Figure 3(b–e). When the nozzle distance was increased, the interaction of the electric field decreased, and this resulted in enhanced electrostatic force on each bubble. As a result, the bubbles were stretched higher at a faster frequency. Therefore, the productivity of the nanofiber increased with increasing nozzle distance. There were two views of the bubbles formed on the top surface of two nozzles during double-nozzle air-jet electrospinning. One view revealed that the bubbles appeared simultaneously on the top surface of the two nozzles [Figure 3(f)]. The other view showed that bubbles appeared intermittently on the top surface of the two nozzles [Figure 3(g)]. The experiments showed that bubbles usually appeared intermittently on the top surface of the two nozzles. For these reasons, the phenomenon of jet repulsion during multineedle electrospinning could be prevented with this double-nozzle air-jet electrospinning device; this contributed to the formation of a continuous and even thickness of the nanofiber webs.[22]

Figure 4 shows the nanofiber webs from the double-nozzle air-jet electrospinning collected at different nozzle distances for 10 min. When the nozzle distances were 20 and 40 mm, nanofiber webs with a continuous and even thickness were obtained [Figure 4(a)]. This result could be explained by the strong interaction of the electric field [Figure 2(a)] and the reduced jet repulsion caused by the intermittently ruptured bubbles on the two nozzles [Figure 3(g)]. When the nozzle distance increased from 20 to 40 mm, the deposition of the nanofiber web was still continuous, but the center distance of the nanofiber web from each nozzle increased [Figure 4(b)]. When the nozzle distance exceeded the critical distance of 55 mm, the nanofiber web began to separate into two parts, as shown in Figure 4(c,d). This was due to the separated equipotential lines, which indicated a weakened electric field in the middle of the two-nozzle plane [Figure 2(c,d,g,h)].

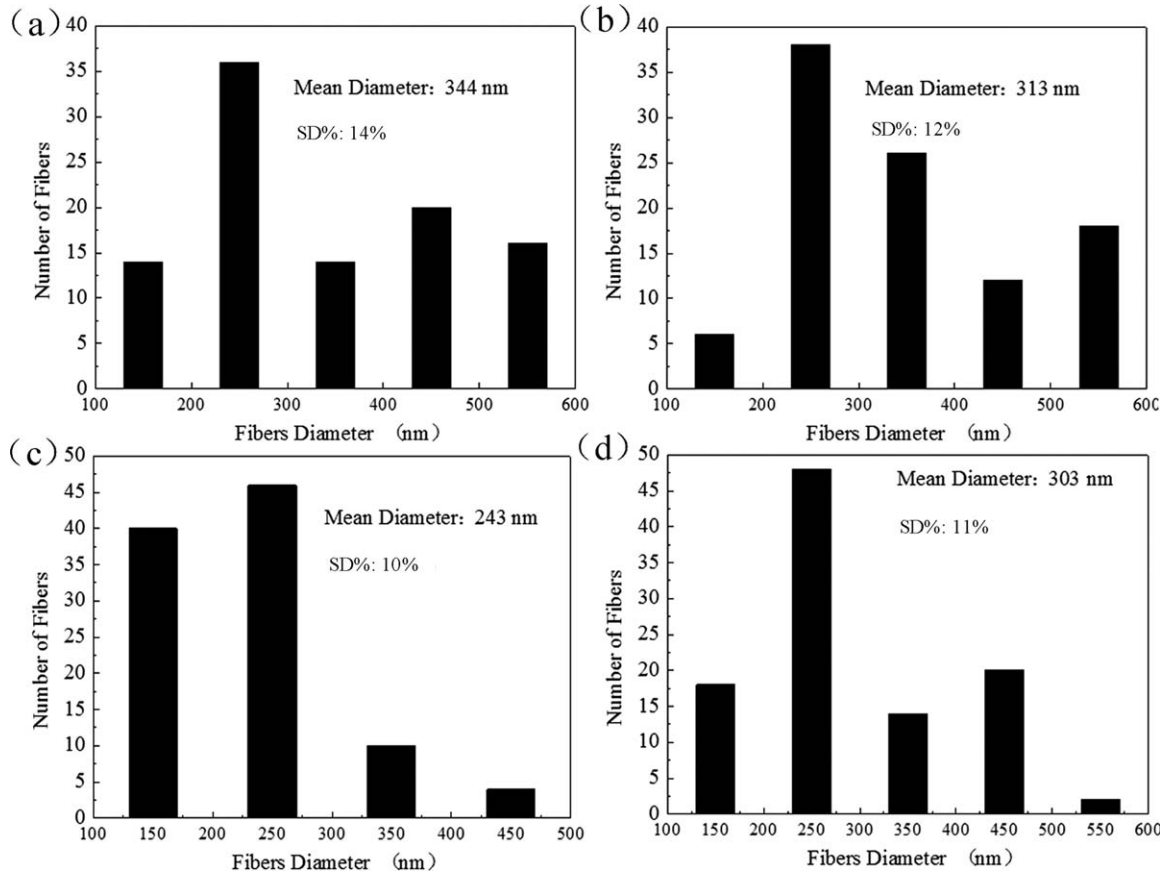

Figure 11. Histograms showing the size distributions and SDs of the nanofibers produced at collecting distances of (a) 14, (b) 16, (c) 18, and (d) 20 cm.

However, the separated nanofiber webs were produced during multineedle electrospinning as a consequence of repulsion from neighboring jets.[23]

Figure 5 shows the deposition areas and the productivity of nanofiber webs collected at different nozzle distances for 1 h. As shown in Figure 5, with the increase in the nozzle distances, both the productivity and deposition area of the nanofiber webs increased. This behavior was caused by the gradually enlarged electric field on the top of each nozzle due to the decreased interaction of the electric field (Figure 2). For comparison, an SNE setup was used to produce PAN nanofibers with the same polymer solution. The maximum productivity of the webs produced by the SNE setup was shown to be about 106 mg/h. The results show that the setup we proposed provided an increased production rate nearly 70 times larger than that found with the SNE setup.

Figure 6 shows the SEM micrographs of the nanofibers electrospun at different nozzle distances. The average diameter and SD of the nanofibers are shown in Figure 7. We found that the average diameter of the nanofibers decreased from 333 to 236 nm with increasing nozzle distance. This could be explained by the enhanced electric field intensity on the top of each nozzle, as shown in Figure 2. The SD of nanofiber was found to decrease from 20 to 10% when the nozzle distance was increased from 20 to 55 mm, and the SD increased again to 14% when the nozzle distance was further increased to 65 mm. This could be illustrated by the most uniform distribution of the electric field at a nozzle distance of 55 mm, as illustrated in Figure 2(c,g).

Effects of the Experimental Parameters

The SEM images of the nanofibers at different applied voltages are shown in Figure 8, and the average diameters and SDs of the nanofibers are shown in Figure 9. The collecting distance was set as 18 cm, and the air flow rate was 800 mL/min. When the applied voltage varied from 36 to 24 kV, the nanofiber diameter was found to increase linearly from 247 to 308 nm, and the SD increased from 10 to 18%. With the decrease in the applied voltage, the nanofibers were stretched incompletely by the weakened electric force; this resulted in thicker and more nonuniform nanofibers. In particular, at an applied voltage of 36 kV, the nanofibers presented the thinnest diameter of 247 nm because of the strongest electric field density, and the SD decreased to its lowest value of 10%.

The collecting distance was changed to show its effect on the nanofiber morphology. SEM images of the nanofibers are shown in Figure 10; the average diameters and SDs of the nanofibers are shown in Figure 11. When the collecting distance changed from 14 to 16 cm, the average diameter of the fibers distributed from 344 to 313 nm, and the SD ranged from 14 to 12% [Figure

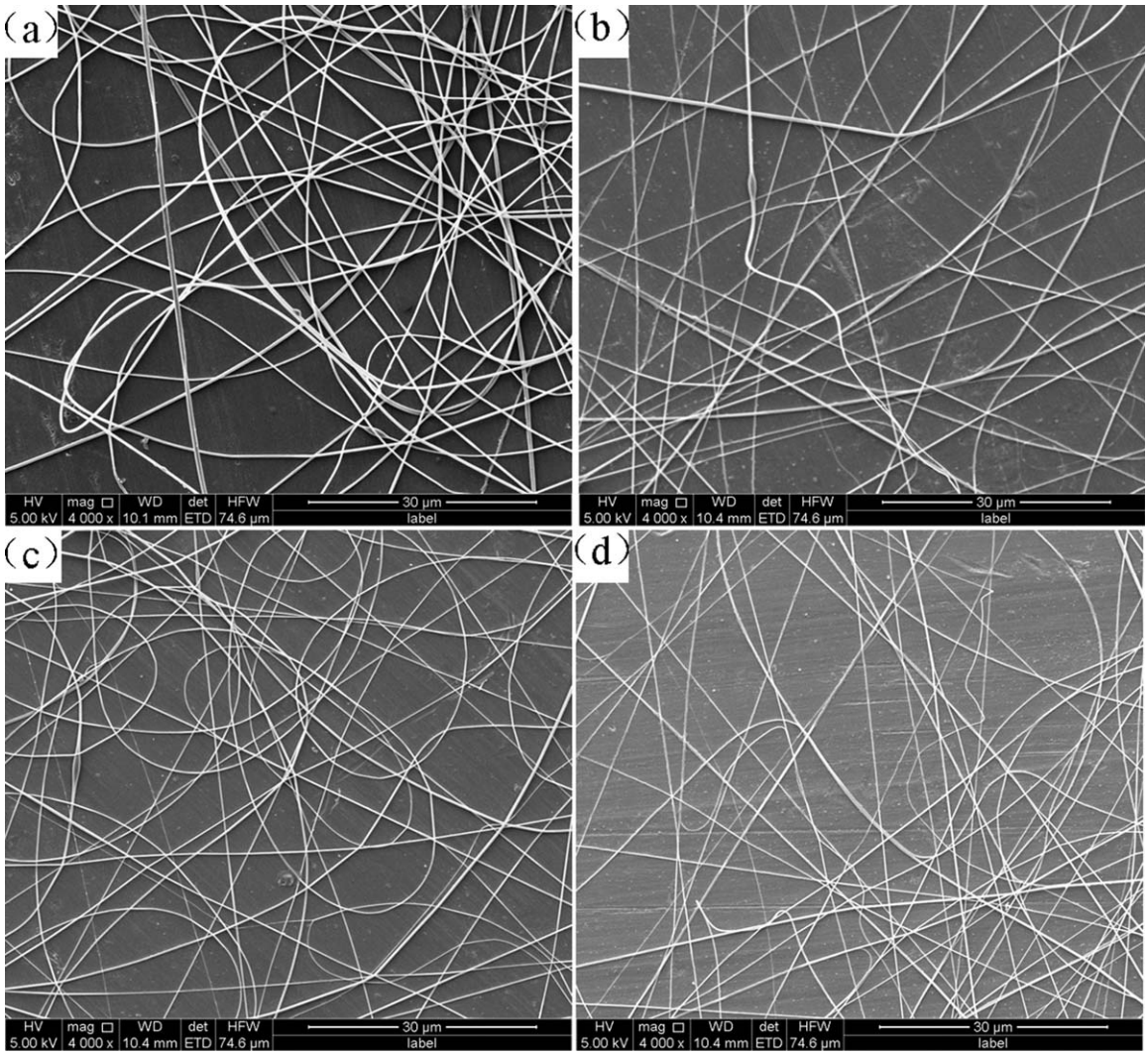

Figure 12. SEM micrographs of nanofibers produced at air flow rates of (a) 400, (b) 600, (c) 800, and (d) 1000 mL/min.

11(a,b)]. This may have been because the fibers were stretched incompletely before they reached the collector; this resulted in thicker and nonuniform fibers. However, when the collecting distance increased from 16 to 18 cm, the average diameter of the nanofibers decreased obviously to a higher level of 243 nm, and the SD decreased to 10% [Figure 11(b,c)]. This could be explained by the fact that the larger working distance may have enhanced the jet flight time and solvent evaporation. When the collecting distance increased to 20 cm, the average diameter of the fibers increased again to 303 nm, and the SD increased to 11% [Figure 11(d)].

The flow rate of air is a critical parameter for air-jet electrospinning because the flow rate of air determines the frequency and the size of the bubbles, which will affect the nanofiber morphology and productivity. Figure 12 shows the SEM images of nanofibers at different air flow rates. The average diameters and SDs of the nanofibers are shown in Figure 13. At a lower air flow rate of 400 mL/min, the average diameter of the nanofibers was the thickest with a larger distribution [Figures 12(a) and 13(a)]. At a lower air flow rate, the bubble burst into larger drops with a thicker and nonuniform diameter. The diameter of the obtained nanofibers remained thin and uniform until the flow rate of air was increased to 800 mL/min [Figure 13(a–c)]. When the flow rate of air was increased from 400 to 800 mL/min, the average diameter of the nanofibers decreased from 384 to 244 nm, and SD decreased from 15 to 9% [Figure 13(a–c)]. As the flow rate of air increased, the bubbles formed with a thin wall and burst into smaller drops, which were stretched into thinner and more uniform nanofibers. In addition, the enlarged internal pressure of the ruptured bubbles caused by the increased air flow rate also contributed to thinner nanofibers. At an air flow rate of 1000 mL/min, the average diameter of the nanofibers increased again to 303 nm, and the SD increased again to 11% [Figure 13(d)]. With the increase in the air flow rate, the formed bubble could overlap with the following ones, and this led to the formation of larger drops.

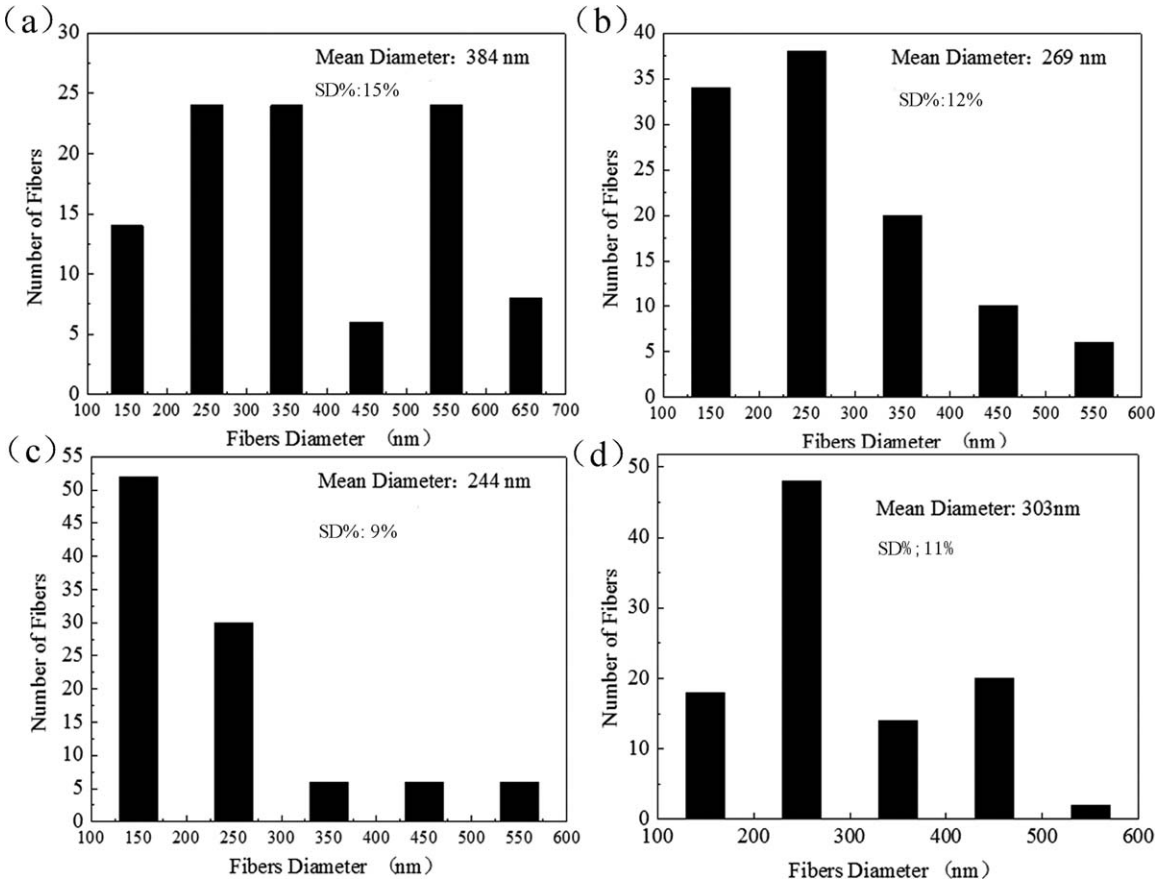

Figure 13. Histograms showing the size distributions and SDs of the nanofibers at air flow rates of (a) 400, (b) 600, (c) 800, and (d) 1000 mL/min.

CONCLUSIONS

To improve the production rate of nanofibers, a novel double-nozzle air-jet electrospinning setup was designed. The distribution of the electric field of this electrospinning system was simulated when the nozzle distances were changed from 20 to 65 mm. The effects of the electric field on the jet path, productivity, deposition area of the nanofiber webs, and nanofiber morphology were also investigated. The results show that continuous and round nanofiber webs were obtained when the nozzle distance was less than 55 mm. When the nozzle distance was changed from 20 to 65 mm, the nanofibers diameter increased from 333 to 236 nm, and the SD of nanofibers was the lowest at 18% when the nozzle distance was 55 mm. In addition, the deposition area and the productivity of the nanofiber was shown to increase with increasing nozzle distance. Furthermore, at a nozzle distance of 55 mm, the effects of the electrospinning parameters, including the applied voltage, collecting distance, and air flow rate, on the nanofiber morphology were also investigated. The results show that the obtained fibers are more uniform with smaller diameter at the applied voltage of 36 kV, the collecting distance of 18 cm and the flow rate of air of 800 ml/min.

ACKNOWLEDGMENTS

This work was supported by a grant from National Natural Science Foundation of China (contract grant number 51203196). The financial support of the United Foundation of the National Natural Science Foundation of China and The People's Government of Henan Province for Cultivating Talents (contract grant number U1204510) is gratefully acknowledged.

REFERENCES

1. Chronakis, I. S. *J. Mater. Process. Tech.* **2005**, *167*, 283.
2. Subbiah, T.; Bhat, G. S.; Tock, R. W.; Parameswaran, S.; Ramkumar, S. S. *J. Appl. Polym. Sci.* **2005**, *96*, 557.
3. Zhou, F. L.; Gong, R. H.; Porat, I. *Polym. Int.* **2009**, *58*, 331.
4. Tomaszewski, W.; Szadkowski, M. *Fiber. Text. East. Eur.* **2005**, *13*, 22.
5. Varesano, A.; Rombaldoni, F.; Mazzuchetti, G.; Tonin, C.; Comotto, R. *Polym. Int.* **2010**, *59*, 1606.
6. Ding, B.; Kimura, E.; Sato, T.; Fujita, S.; Shiratori, S. *Polymer* **2004**, *6*, 1895.
7. Fong, H.; Chun, I.; Reneker, D. H. *Polymer* **1999**, *16*, 4585.
8. Varesano, A.; Carletto, R. A.; Mazzuchetti, G. *J Mater. Process. Tech.* **2009**, *209*, 5178.
9. Angammana, C. J.; Jayaram, S. H. *IEEE Trans. Ind. Appl.* **2011**, *47*, 1028.
10. Liu, L. H. Studies on the deposition and alignment of electrospun nanofiber assemblies. Ph.D. Thesis, University of Nebraska, Yuris A. D. December **2006**.

11. Kim, G. H.; Cho, Y. S.; Kim, W. D. *Eur. Polym. J.* **2006**, *42*, 2031.
12. Deitzel, J. M.; Kleinmeyer, J. D.; Hirvonen, J. K.; Tan, N. C. *Polymer* **2001**, *2*, 8163.
13. Niu, H. T.; Wang, X. G.; Lin, T. *J. Eng. Fiber. Fabr.* **2012**, Special Issue, 17.
14. Kostakova. E,; Meszaros, L.; Gregr, J. *Mater. Lett.* **2009**, *63*, 2419.
15. Wang, X.; Niu, H.; Wang, X.; Lin, T. *Polym. Eng. Sci.* **2009**, *49*, 1582.
16. Niu, H. T.; Lin, T.; Wang, X. G. *J. Appl. Polym. Sci.* **2009**, *114*, 3524.
17. Kim, J. S.; Reneker, D. H. *Polym. Eng. Sci.* **1999**, *39*, 849.
18. Yang, R. R.; He, J. H.; Xu, L.; Yu, J. Y. *Polymer* **2009**, *50*, 5846.
19. Tang, S.; Zeng, Y.; Wang, X. *Polym. Eng. Sci.* **2010**, *50*, 2252.
20. Bird, J. C.; Ruiter, R. D.; Courbin, L.; Stone, H. A. *Nature* **2010**, *465*, 759.
21. Baumgarten, P. K. *J. Colloid Interface Sci.* **1971**, *36*, 71.
22. Angammana, C. J.; Jayaram, S. H. *IEEE Trans. Ind.* **2011**, *47*, 1028.
23. Kumar, A.; Wei, M.; Barry, C.; Chen, J. *Macromol. Mater. Eng.* **2010**, *295*, 701.